

P Kang
KKH Svoboda

Nicotine inhibits palatal fusion and modulates nicotinic receptors and the PI-3 kinase pathway in medial edge epithelia*

Authors' affiliations:

Pei Kang, Kathy K.H. Svoboda,
Biomedical Sciences, Texas A & M University
System, Baylor College of Dentistry, Dallas,
TX, USA

Correspondence to:

Kathy K.H. Svoboda
Biomedical Sciences Department
Baylor College of Dentistry
3302 Gaston Ave
Dallas, TX 75246, USA
Tel.: 214 828 8487
Fax: 214 828 8951
E-mail: ksvoboda@tambcd.edu

Dates:

Accepted 12 December 2002

To cite this article:

Orthod Craniofacial Res 6, 2003; 129–142
Kang P, Svoboda KKH.
Nicotine inhibits palatal fusion and modulates
nicotinic receptors and the PI-3 kinase pathway
in medial edge epithelia

*This work was supported by, Grant Sponsor:
Baylor Oral Health Foundation; NIH (Grant No.:
EY-08886); Tobacco Endowment Fund,
Texas A & M University System (Grant No.:
304-202850-4013).

Copyright © Blackwell Munksgaard 2003
ISSN 1601-6335

Structured Abstract

Authors – Kang P, Svoboda KKH

Objectives – To analyze the effects of nicotine on palatal fusion inhibition *in vitro* and determine if nicotine modulated transforming growth factor β 3 or phosphatidylinositol-3 kinase signaling. A second objective was to determine the localization and regulation of nicotinic receptors in the medial edge epithelia (MEE) during palatal fusion.

Design – Palatal shelves from embryonic day (E) 13.5 mice were cultured in serum free media and treated with 0, 0.06, 0.6, or 6 mM nicotine, nicotinic receptor antagonist α -bungarotoxin, or the combination of nicotine and α -bungarotoxin. Tissues harvested at 72 h were analyzed for epithelial-mesenchymal transformation (EMT) and fusion. MEE samples collected at 20 h were analyzed for phosphorylated Akt-Ser473, phosphorylated Smad2, and nicotinic receptors.

Results – Nicotine inhibited palatal fusion *in vitro* in a dose dependent manner. Activated Akt-Ser473 was greater in control MEE than in nicotine treated tissues; while there was no difference in activated Smad2 between groups. The α 7 subunit of nicotinic receptor was expressed in MEE during palate fusion and increased in nicotine treated tissues. Alpha-bungarotoxin did not rescue the nicotine treated palates.

Conclusion – Nicotine treatment had no effect on Smad2, but caused a down regulation of the PI-3 kinase pathway that may have contributed to inhibiting palatal fusion *in vitro*.

Key words: Akt; epithelial-mesenchymal transformation; nicotine; palate; phosphatidylinositol-3 kinase; Smad

Introduction

It is generally accepted that exposure to nicotine has adverse effects on fetal development. Higher mortality

rates and lower birth weights are associated with maternal smoking during pregnancy (1–3). Animal studies have shown that nicotine administration during pregnancy resulted in delayed implantation and decreased fetal weight (4), abnormal incisor and molar formation (5, 6), and delayed tongue development (7). Maternal cigarette smoking as a risk factor for cleft palate has been demonstrated by epidemiological studies (8–10). In addition, fetal cleft palates can be induced in goats by maternal gavage of *nicotiana glauca* (11, 12). Cleft palate was also induced in mice by daily maternal nicotine hemisulfate injections from gestational days 6–15 (13).

Normal palatal development requires multiple cell–cell interaction and procedures. Two palatal shelves initially project vertically from the maxillary processes into the oral cavity on embryonic day 12 (E12) in mice and grow on both sides of the tongue. The palatal shelves reorient to a horizontal position superior to the tongue (E13 in mice) and grow to meet in the midline (14, 15). Palatal shelves are composed of craniopharyngeal ectoderm and neural crest derived mesenchyme (16). At these early developmental stages, two epithelial layers cover the developing palatal shelves, the superficial periderm and the basal epithelium. The periderm sloughs off and exposes the basal layer prior to the adherence of opposing palatal shelves (17). Basal epithelia of the medial edges of the contacting shelves form new desmosomes on the apical surface and adhere one another to form an epithelial seam (18). The seam epithelia thin to one layer and divide into islands. They eventually disappear, resulting in the final confluence of the mesenchyme and complete fusion of the palate (14, 19). In the investigation of medial edge epithelia (MEE) disappearance and resulting mesenchymal confluence, several studies suggested that most of the MEE, if not all, go through epithelial–mesenchymal transformation (EMT) (18, 20, 21). During this phenotypic change, MEE lose cell–cell adhesion, change cell shape, degrade the basement membrane, and migrate into mesenchyme. At the same time as MEE transform into mesenchyme, the epithelia on the oral surface become masticatory mucosa, while the epithelia on the nasal surface differentiate into pseudostratified ciliated columnar cells lining the airspace. Disturbances at any stage during this process, i.e., defective palatal shelf growth, failed or delayed shelf elevation, or failure of EMT and fusion can result in cleft palate.

Many biological agents regulate EMT during palate development. There are numerous experiments that support the hypothesis that transforming growth factor (TGF) β 3 contributes to palatal fusion (22–25). Tgf β 3 and type II Tgf β receptors (T β R-II) are localized in the MEE before fusion (26). Tgf β 3 transgenic and knockout mice have cleft palate as their only craniofacial birth defect (22, 23). When palatal shelves from Tgf β 3 knockout mice were cultured, the midline epithelia failed to go through EMT (24). The addition of TGF β 3 into culture media rescued the fusion of the palates from Tgf β 3-null mice (25). Interestingly, although chickens have naturally open palates, the cultured palatal shelves fused when TGF β 3 was added into the media (27).

Some of the TGF β 3 downstream signaling molecules are included in the Smad family (28, 29). Although Smad expression was detected during palatal fusion (30), they have not been proven to be essential factors for EMT. Phosphatidylinositol-3 (PI-3) kinases an alternative downstream signal in the TGF β pathway as it is involved in actin reorganization, matrix metalloproteinases (MMP) production, and cell mobility (31, 32). Recently, we have demonstrated that LY294002, a specific inhibitor of PI-3 kinase, blocked EMT and palate fusion *in vitro* (33).

There is evidence that nicotine regulates the production and release of fibroblast growth factor (FGF), TGF β , and extracellular matrix in smooth muscle cells (34, 35) and vascular endothelial cells (36). Whereas, nicotine modulates EGF and TGF β in cervical cancer cells (37, 38). Therefore, if nicotine inhibits EMT and palate fusion, it is important to determine the effects of nicotine on growth factors and signaling pathways involved in palate development, such as TGF β 3 and PI-3 kinase.

It is generally recognized that in the neural system, nicotine elicits its effects by interacting with nicotinic acetylcholine receptors (nAChRs). These receptors are also localized in epithelial cell populations (39, 40). Nicotine regulates the expression of nAChRs subunits and the receptors are involved in modulating cell shape, motility, proliferation and differentiation (39–42). We hypothesize that if nAChRs are present in MEE during palate development, they mediate the toxic effects of smoking.

In the current study, we investigated if nicotine inhibits EMT and palatal fusion *in vitro* and if the effect is regulated through TGF β 3 or PI-3 kinase signaling.

We also studied the localization and regulation of nAChRs in MEE during EMT and palatal fusion.

Materials and methods

Embryos

Timed-pregnant CD 1 mice (Harlan Sprague Dawley Inc., Indianapolis, IN, USA) were used in these studies. Animals were maintained under standard conditions at a 10 h:14 h light:dark cycle. Female mice were mated overnight and the day of vaginal plug was timed as day 0. In CD 1 mice, the palate shelves elevate above the tongue between E13 and E13.5 days. Therefore, pregnant females were killed by cervical dislocation at 13.5 day and the embryos were dissected out of the amniotic sacs into a dish of ice-cold Hanks' balanced salt solution (HBSS; Gibco, Grand Island, NY, USA). The stage of development was determined using morphological features.

CCFSE labeling of palate shelves

The surface epithelia were labeled with (5 and 6) carboxy 2,7' dichlorofluorescein diacetate succinimidyl ester (CCFSE; Molecular Probes) according to the methods of Griffith and Hay (43). Briefly, 1:500 dilution of 10 mM CCFSE stock solution (in dimethyl sulphoxide, DMSO) was prepared in HBSS and warmed at 37°C prior to use. After mandibles and tongues were removed from the embryos, upper heads were exposed to CCFSE for 1.5 h at 37°C. For controls, tissues were exposed to DMSO under the same conditions. The upper heads were then rinsed in HBSS to remove the unincorporated CCFSE followed by dissection and organ culture of the palatal shelves. At the completion of the experiment, the whole palates were evaluated with confocal microscopy. Complete z-series were obtained, and representative signal optical images from the EMT region were used for figures.

Organ culture and treatment with PI-3 kinase inhibitor

Palatal shelves were dissected from E13.5 mouse embryos and placed nasal side down on HATF filters (0.45 μ m pore size; Millipore Corp., Bedford, MA, USA) with their medial edges in contact. The tissues were suspended at the air-media (BGJb; Gibco) interface on a

triangular-shaped wire grid in an organ culture dish. Nicotine treated groups were supplemented with nicotine hemisulfate (Sigma, St Louis, MO, USA) at concentrations of 0.06, 0.6, or 6 mM. α -bungarotoxin (α -BTX) was added at 1 or 10 μ M (Sigma). In the groups treated with both nicotine and antagonist, tissues were incubated with α -BTX for 1 h at 37°C before both nicotine and α -BTX were added into the media. The medium barely covered the apical surface of the palates. Tissues were incubated at 37°C in a humidified gas mixture (5% CO₂ and 95% air) and media was changed every 24 h. Experiments were repeated 16 times with a total of 120 embryos from 22 pregnant mice.

Histology and immunohistochemistry

Cultured palatal shelves collected at 72 h were fixed in freshly prepared 4% paraformaldehyde/phosphate-buffered saline (PBS) (pH = 7.4) for 30 min. After rinsing in PBS, the tissues were processed for paraffin embedding. Serial sections (8 μ m thickness) were collected and numbered in sequence from rostral to caudal. Light microscopic analysis of hematoxylin and eosin stained sections (H and E) was completed and a Zeiss Axioplan was used to capture images. Serial sections were also evaluated for the expression of laminin. After blocking with 10% normal goat serum/PBS, the tissues were incubated in 1:30 rabbit anti-laminin (Sigma) for 2 h at room temperature except for negative controls. Following rinsing, the primary antibody was detected by 1:100 fluorescein isothiocyanate conjugated goat-anti-rabbit antiserum (Jackson Immuno-Research, PA, USA).

Samples harvested at 20 h were infiltrated in 50/50 PBS/ornithine carbamoyl transferase embedding medium (Sakura Finetec, CA, USA) for 5 min before being mounted as frozen blocks and stored in -80°C freezer. Serial 8 μ m coronal sections were collected and fixed in acetone at -20°C for 20 min. After blocking with 10% goat serum, the samples were incubated overnight at 4°C in 1:100 primary antibodies (phosphorylated Akt-Ser473, Santa Cruz Biotechnology, CA, USA; phosphorylated Smad2-Ser 465/467, Upstate Biotechnology, NY, USA; α -7 nicotinic receptor subunit, Biodesign International, ME, USA) in 3% goat serum except negative controls. Following rinsing, the primary antibody was detected by 1:100 Alexa Fluor® 488 goat-anti-rabbit antiserum (Molecular Probes, OR, USA).

After mounting in SlowfadeTM media (Molecular Probes, Eugene, OR, USA), the images were obtained using a Leica SP2 confocal microscope. All treatment groups were viewed at the same settings for each antibody. All secondary antibody controls were negative. Images were arranged with Adobe Photoshop and PageMaker programs, with careful attention to equal image enhancement for all treatment groups.

Fluorescent α -bungarotoxin labeling

Cryostat sections were collected and fixed as described above. Slides were then incubated with 1:75 Alexa Fluor[®] 488 α -bungarotoxin (α -BTX; Molecular Probes) for 1.5 h at 37°C. Negative control was incubated in Alexa Fluor[®] 594 α -BTX in the same conditions. After rinsing and mounting in SlowfadeTM media, the images were obtained using a Leica SP2 confocal microscope with an excitation wavelength of 488 μ m. All treatment groups were analyzed at the same microscope settings on the same day and arranged with Adobe Photoshop and PageMaker programs.

Confocal laser scanning microscopy

Immunohistochemical experiments and α -BTX labeling were analyzed with the Leica upright TCS-SPII confocal microscope, equipped with argon and helium neon lasers with excitation wavelengths of 457, 488, 514, 543 and 633 μ m. The tissues were analyzed with 10 \times and 20 \times air lenses. *En face* images of the carboxyfluorescein labeled whole mount palates were obtained from oral to nasal epithelia at approximately 3- μ m intervals. Optical images from representative depths were analyzed, enhanced and stored. Images were arranged with Adobe Photoshop and PageMaker programs.

Western blot analysis

Cultured palatal shelves were harvested at 20 h (n = 15 palates/treatment group/experiment). Tissues from different experiments (n = 4) were kept separately. To reduce the contamination by mesenchyme, the middle 1 mm (0.5 mm on either side of the MEE) of the palates were dissected and placed in lysis buffer (10 mM Tris buffer, 150 mM NaCl, 1 mM ethylenediaminetetraacetic acid, 0.1% TX100, and 0.1% NP40) with 1% protease inhibitor, phosphatase inhibitor

cocktails I and II (Sigma-Aldrich, St. Louis, MO, USA). The tissues were then sonicated and centrifuged at 20,800 g for 30 min and the resultant supernatant was saved. Duplicate aliquots of each sample were used for Lowry assays to determine protein concentration. Proteins were separated on 7.5% sodium dodecyl sulphate-polyacrylamide gel electrophoresis pre-cast gels (Bio-Rad, Hercules, CA, USA) and transferred onto Immobilon-P polyvinylidene fluoride (PVDF) membranes (Millipore, Billerica, MA, USA). The non-specific binding sites on the membranes were blocked by incubating in blocking buffers: 2% BSA-Tris-buffered saline with 0.1% Tween 20 (TBST) for phosphorylated antibodies for 1 h at room temperature; and 5% milk-TBST for α -7 nicotinic receptor subunit (α -7AChR) antibody overnight at 4°C. This was followed by 12-h incubation in primary antibodies at 4°C (1:100 Akt/2% BSA-TBST; 1:500 Smad2/5% milk-TBST; 1:800 nicotinic receptor/5% milk-TBST). After rinsing in TBST, membranes were incubated in secondary antibodies conjugated with horseradish peroxidase for 1–2 h at room temperature. Proteins were detected using femtoLucentTM sans (Geno Technology Inc., MO, USA) and probes were observed on Kodak Image station 440_{CF} (Eastman Kodak Digital ScienceTM, Rochester, NY, USA). Images were arranged with Adobe Photoshop and with PageMaker programs. Experiments were repeated twice from separate litters and the Western blots were analyzed with densitometry. The mean densitometry value was graphed.

Palatal fusion stages

The palates went through different degrees of EMT and fusion after 72 h *in vitro*. Five stages of fusion (1–5) were scored according to confocal and histo-morphological observations (33). We calculated the mean fusion score (MFS) by taking the stage (1–5) times the number of embryos, and divided the sum by the total number of embryos in that group. For example, to calculate the MFS for the controls the following calculation was made: [(1)(3) + (5)(4) + (16)(5)]/22 = 4.67 (Table 1). Therefore groups with more complete palatal fusion had MFS closer to 5. MFS was compared between groups using Kruskal–Wallis test, a non-parametric test (distribution-free) used to compare three or more independent groups of sampled data. *p*-Value of <0.01 was considered statistically significant.

Table 1. Stages of palatal shelf fusion and MFS in different treatment groups

Stages of fusion/treatment	Non-fusion		Partial fusion	Complete fusion		Total	MFS
	1	2		4	5		
Control	0	0	1	5	16	22	4.67
0.06 mM nicotine	0	0	0	1	3	4	4.75
0.6 mM nicotine	0	0	8	1	0	9	3.11*
6 mM nicotine	23	3	0	0	0	26	1.16*
1 μ M α -BTX	0	0	1	2	6	9	4.56
10 μ M α -BTX	0	0	1	1	4	6	4.50
1 μ M α -BTX + 6 mM nicotine	5	0	1	0	0	6	1.50*
10 μ M α -BTX + 6 mM nicotine	5	0	1	0	0	6	1.50*

*($p < 0.01$) using the Kruskal–Wallis test.

MFS, mean fusion score; α -BTX, α -bungarotoxin.

Results

Palatal tissues were collected from 88 E13.5 mouse embryos using 14 pregnant mice (Table 1). To follow the fate of MEE, a lipophilic marker, CCFSE was used to label the palatal epithelia (43) for confocal analysis. Dissected palatal shelves were placed nasal surface down in pairs with their medial edges in contact in organ culture. Cultures were maintained 20, 48 or 72 h and media were changed daily.

Confocal microscopy was used to examine the overall tissue architecture of cultured palate samples by obtaining complete z-series through the palatal fusion zone. Typical z-series images were obtained from the oral surface to a depth of 1 mm (Levels 1–3 in Fig. 1N) at 3- μ m intervals, and representative sections (Fig. 1A–K) demonstrate that CCFSE could be used to label the surface epithelia and medial edge epithelium (MME). As the MEE transformed into mesenchyme the label became weaker (Fig. 1K–M). The nasal surface was not reached due to the thickness of the tissues (Approximately 1.5 mm).

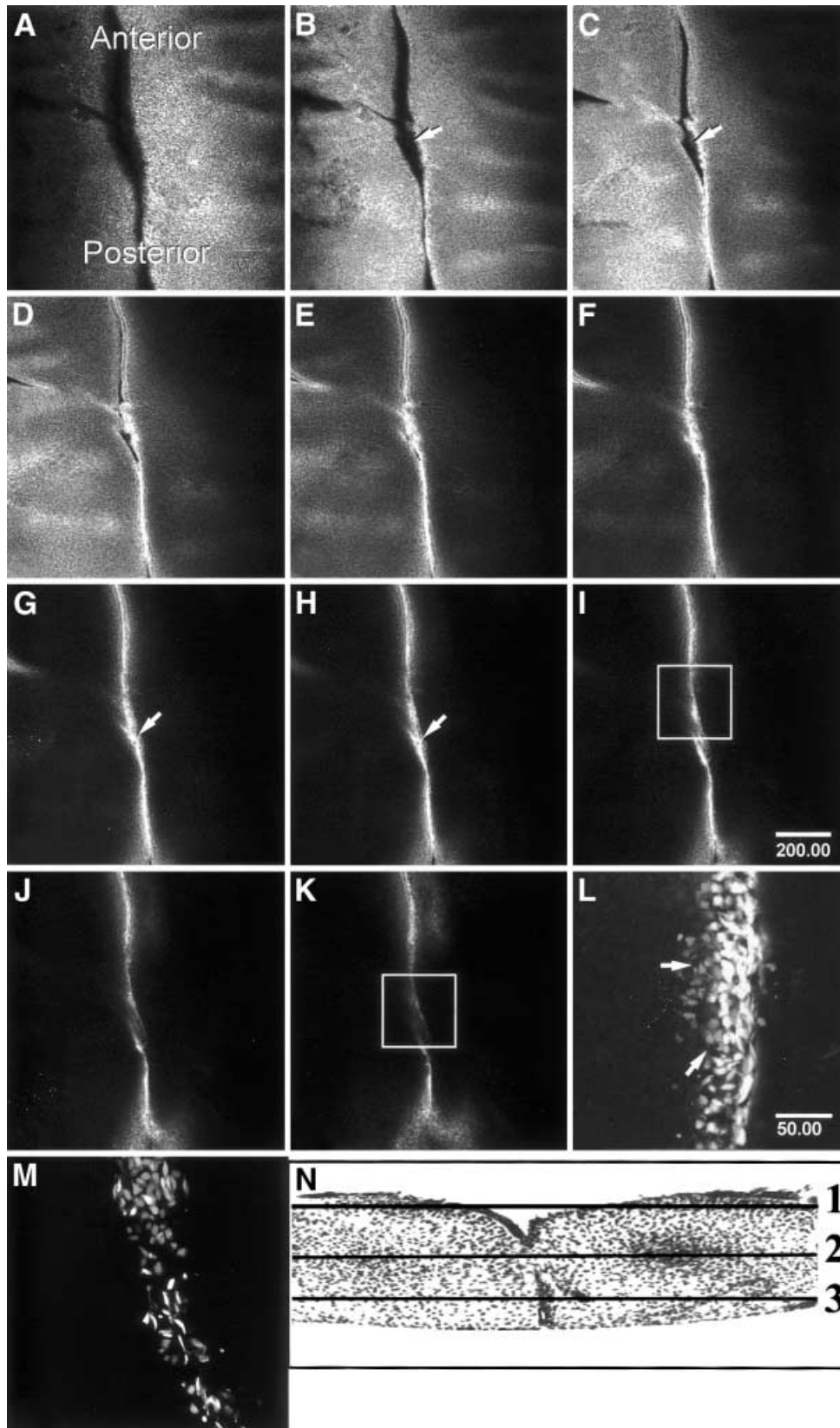
One example of the data obtained from a complete z-series from a control palate cultured for 48 h demonstrated that the oral surface epithelium (Level 1, Fig. 1N) was uniformly labeled with CCFSE (Fig. 1A–D). The palatal shelves were not apposed in the apical sections (Fig. 1A–D), similar to (Level 1, Fig. 1N). The cleft between the two palatal shelves did not contain CCFSE stained tissues and appears as a black area (arrows, Fig. 1B, C). In optical sections toward the

middle of the tissue (Level 2, Fig. 1N), only midline epithelia in the fusion zone were intensely labeled (Fig. 1, F–H). These epithelia adhered and thinned into a single layer from anterior to posterior (arrows, Fig. 1G, H). The midline epithelia (Boxed area in Fig. 1I, K) were examined with higher magnification (Fig. 1L, M) to illustrate that increased space between the labeled epithelial cells was observed. These cells had lost cell–cell adhesion, changed cell shape, and were migrating lateral into the pre-existing mesenchyme (arrows, Fig. 1L, M). Confocal analysis was more informative than paraffin section analysis for overall detection of EMT throughout the palatal cultures. However, the cross sectional data obtained from H & E staining and immunohistochemistry (Fig. 2D, G) provided additional important information concerning the tissue structure (Fig. 2D–F) and basement membrane proteins (Fig. 2G–I).

Control palates ($n = 21/22$) completely fused (16 stage 5, and five stage 4) for a mean fusion score (MFS) of 4.67 by 72 h (Table 1). The labeling was more discretely distributed in the fusion zone (arrows, Fig. 2A) than at 48 h (arrows, Fig. 1L, M), indicating the 72-h cultured palates had achieved mesenchymal confluence and fusion. Palatal shelves cultured with 0.06 mM nicotine progressed through normal EMT and achieved stages 4 or 5 with a MFS of 4.75 after 72 h (Table 1). Whereas, palates treated with 0.6 mM nicotine had intensely CCFSE labeled midline epithelia that were continuous along the fusion zone after 48 h of culture (data not shown). Persistent

midline epithelia were also observed after 72 h in the presence of 0.6 mM nicotine (Fig. 2B, mee), although the seam appeared broken at a few places along the

midline (arrowheads, Fig. 2B). These palate samples were scored as partially fused (stage 3). We also observed one of nine analyzed tissues achieved stage 4



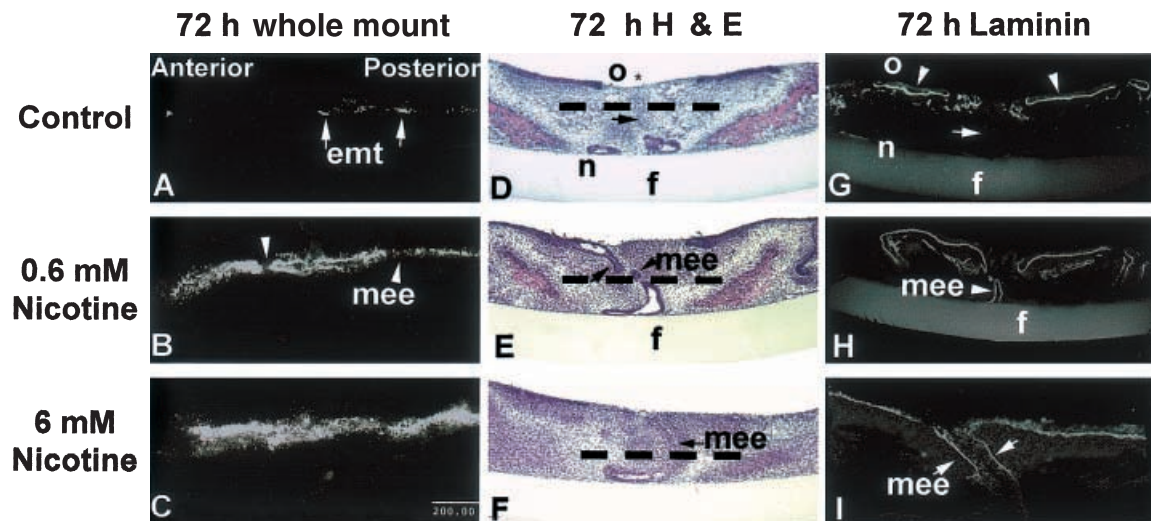


Fig. 2. Analysis of palates after 72 h of culture with or without nicotine treatment. (A–C) Single optical confocal sections through carboxy 2,7' dichlorofluorescein diacetate succinimidyl ester (CCFSE) labeled whole mount palatal tissues in the middle of the tissue, 120 μm from the oral surface, as illustrated by the dashed line in (D–F). (D–F) H and E stained cross sections of samples after 72 h of culture. (G–I) Laminin stained cross sections of tissues cultured for 72 h. Control palates had transformed medial edge epithelia (MEE) demonstrated by decreased CCFSE staining (arrowheads, A), lack of midline epithelia in H and E stained sections (arrow, D), and lack of midline laminin staining (arrow, G). In contrast, palates treated with either 0.6 or 6 mM nicotine had persistent MEE in CCFSE stained optical sections (B, C, arrowheads), midline epithelia in H and E stained sections (arrows, E, F), and positive laminin staining in the midline (arrows, H, I). Medial edge epithelia (mee), epithelial-mesenchymal transformation (emt), oral surface (o), nasal surface (n), filter (f), scale bar = 200 μm .

fusion (Table 1), with only small epithelial islands persisting in the midline. The overall MFS for 0.6 mM nicotine treatment group was 3.11, which was significantly lower ($p < .01$) than the control and 0.06 mM nicotine treatment groups.

In the palates treated with 6 mM nicotine, confocal observations of CCFSE labeling and histochemical analysis demonstrated persistent epithelia in the midline after 48 or 72 h, and mesenchymal confluence was

not achieved (Fig. 2C). Using our scoring protocol, 23 of 26 palates were stage 1. In addition, three samples were scored as stage 2, providing a total MFS of 1.16, significantly ($p < .01$) different from control palatal fusion scores.

Palate fusion and disappearance of MEE in samples cultured for 72 h were confirmed by hematoxylin and eosin (H and E) stained cross sections. No continuous epithelia remained in the midline region (arrow, Fig. 2D) and mesenchyme formed a confluent layer of control samples. We also observed that the epithelia in the medial region of oral surface (o) disappeared in most of the fused palate samples (Asterisk, Fig. 2D). These epithelia were presumably MEE in origin.

The size and thickness of the palatal shelves of the nicotine treated tissues were similar to the control group (Fig. 2D–F); however, proliferation analysis was not completed in the current investigation. In the palate tissues treated with 0.6 or 6 mM nicotine, two distinct layers of cuboidal shaped MEE persisted in the fusion zone on the nasal and oral sides (arrow, Fig. 2E, F). The midline seam was broken but an epithelial island remained (arrowhead, Fig. 2E) in the tissues treated with 0.6 mM, but not 6 mM nicotine.

As breakdown of the basement membrane is a critical step in EMT, we examined the presence of

Fig. 1. (A–M) Single optical images of carboxyfluorescence labeled palatal shelves after 48 h in culture under control conditions. (N) H and E stained palate used to show representative levels of optical sectioning by confocal microscopy from oral surface (Level 1) the middle of the tissue (Level 2), and toward nasal surface (Level 3). Single optical sections from the oral surface to approximately 120 μm depth into the tissues were recorded. Representative images (A–K) were analyzed. Oral surface epithelia were labeled with CCFSE (A, B, C, and D). At these optical planes (N, Level 1), the medial edge epithelia (MEE) (arrows in B and C) did not adhere. Because of tissue tilting during mounting, images from different levels of the palate were captured, which resulted in the slight difference of labeling intensity of the oral epithelia from the two shelves (A, B, and C). In deeper optical sections toward the middle of the tissue (Level 2, N), only MEE were intensely labeled (arrows in G and H). The MEE already thinned into a single seam. In optical planes (J and K) at level 3 (N), broken areas in the seam were detected. In higher magnification (40 \times) image of the boxed areas in (I) and (K) are represented in (L) and (M), respectively. Transformed and migrating epithelial cells were observed in the broken areas of the seam (arrows, L and M) by double labeling with phalloidin. Scale bar = 200 μm in (A–K) and 50 μm in (L–M).

laminin in the cultured palates. Laminin expression was observed under the oral epithelia (arrowheads, Fig. 2G). However, the fusion zones of the control-cultured samples (arrow, Fig. 2G) were negative for laminin, suggesting that the basement membrane of the MEE was completely degraded. Some areas of laminin staining were observed beneath the oral epithelia in both control and nicotine treated palates (Fig. 2G–I). At high magnification some appeared to be the developing blood vessels, while other areas were not identified. In palates treated with nicotine (0.6 or 6 mM) laminin remained in the fusion zone (mee, arrowhead, Fig. 2H and arrows, 2I) demonstrating that the basal lamina had not degraded in these palates. Laminin was detected along the fusion zone (arrows, Fig. 2I), continuous with that of the oral surface epithelia. This result further demonstrated that the MEE did not thin into one layer and the intact basal lamina persisted in the tissues. Therefore, basement membrane degradation, an essential event during EMT, did not occur in nicotine treated palate samples.

In summary, according to our scoring system, the MFS for the 0.6 and 6 mM nicotine treatment groups are 3.11 and 1.16, respectively (Table 1). These values were significantly lower ($p < 0.01$) than the control and 0.06 mM nicotine treatment groups (4.67 and 4.75, respectively). Therefore, in the presence of nicotine, palatal fusion was inhibited in a dose dependent manner.

Signal transduction pathways associated with EMT

As demonstrated by the dose response study, the MEE in control palates was actively transforming into mesenchyme by 48 h and completely transformed by 72 h. To study the signal transduction activation, an earlier time in the EMT process was needed. It was determined that by after 1 day in culture, the palatal shelves had adhered and started to transform, but a substantial population of the MEE remained in the midline (Fig. 3A). Therefore, the tissues were harvested at 20 h to capture the cells in the transforming MEE phenotype. In addition, as the MEE were the focus of the research, cultured palates were either frozen and sectioned for immunohistochemistry or further harvested for Western blot analysis. To enrich the protein

samples for MEE, the midline seam was harvested separately from the whole tissues and pooled by treatment group to obtain enough protein.

Several signaling pathways have been implicated in the EMT process including TGF β 3 (25, 27, 44) and PI-3 kinase (33). PI-3 kinase activates 3-phosphoinositide-dependent protein kinases (PDKs) (45, 46). Integrin-linked kinase (ILK) is a PDK that is involved in EMT, present in the developing palate MEE (47) and phosphorylates Akt on its serine 473 site (48, 49). Smad2 acts as a downstream signaling molecule when TGF β 3 binds to its cell surface receptors. Therefore, the effects of nicotine on PI-3 kinase and TGF β 3 signaling during palate fusion were evaluated by determining the levels of phosphorylated Akt (Ser473) and phosphorylated Smad2 (Ser465/467) by immunohistochemistry (Fig. 3A, B, E, F) and Western blot analysis (Fig. 3C, G).

The midline epithelia were positive for phosphorylated-Akt (Ser473) as observed from a single confocal optical image of a frozen section (Fig. 3A). The fluorescence was discontinuous (arrow, Fig. 3A) and no staining was observed in the fusion zone on the nasal area MEE (asterisk, Fig. 3A), suggesting phosphorylated Akt decreased in the transformed MEE. The palates cultured with 6 mM nicotine had low levels of phosphorylated Akt in the fusion zone (arrow, Fig. 3B) and surface epithelia. Western blot analysis of the middle 1 mm (0.5 mm on either side of the MEE) of the tissues from duplicate experiments confirmed the immunohistochemical results. The phosphorylated-Akt (Ser473) from the control tissues (Fig. 3C, Con) was threefold higher than nicotine treated tissues (Fig. 3C, 6 Nic) in densitometry analysis of duplicate experiments (Fig. 3D).

In contrast, activated Smad2 was not different between controls and nicotine treated palates after 20 h in culture. The MEE stained in a similar pattern and intensity (arrows, Fig. 3E, F) in surface and midline epithelia in both tissues. The discrete fluorescence in the control tissue (asterisk, Fig. 3E) suggested down-regulation of phosphorylated Smad2 in transformed cells. In contrast, activated Smad2 was observed throughout the midline epithelia in 6 mM nicotine treated tissues. Protein analysis demonstrated that nicotine treatment (6 Nic, Fig. 3G) did not alter the level of phosphorylated-Smad2 analyzed by densitometry in duplicate experiments (Fig. 3H).

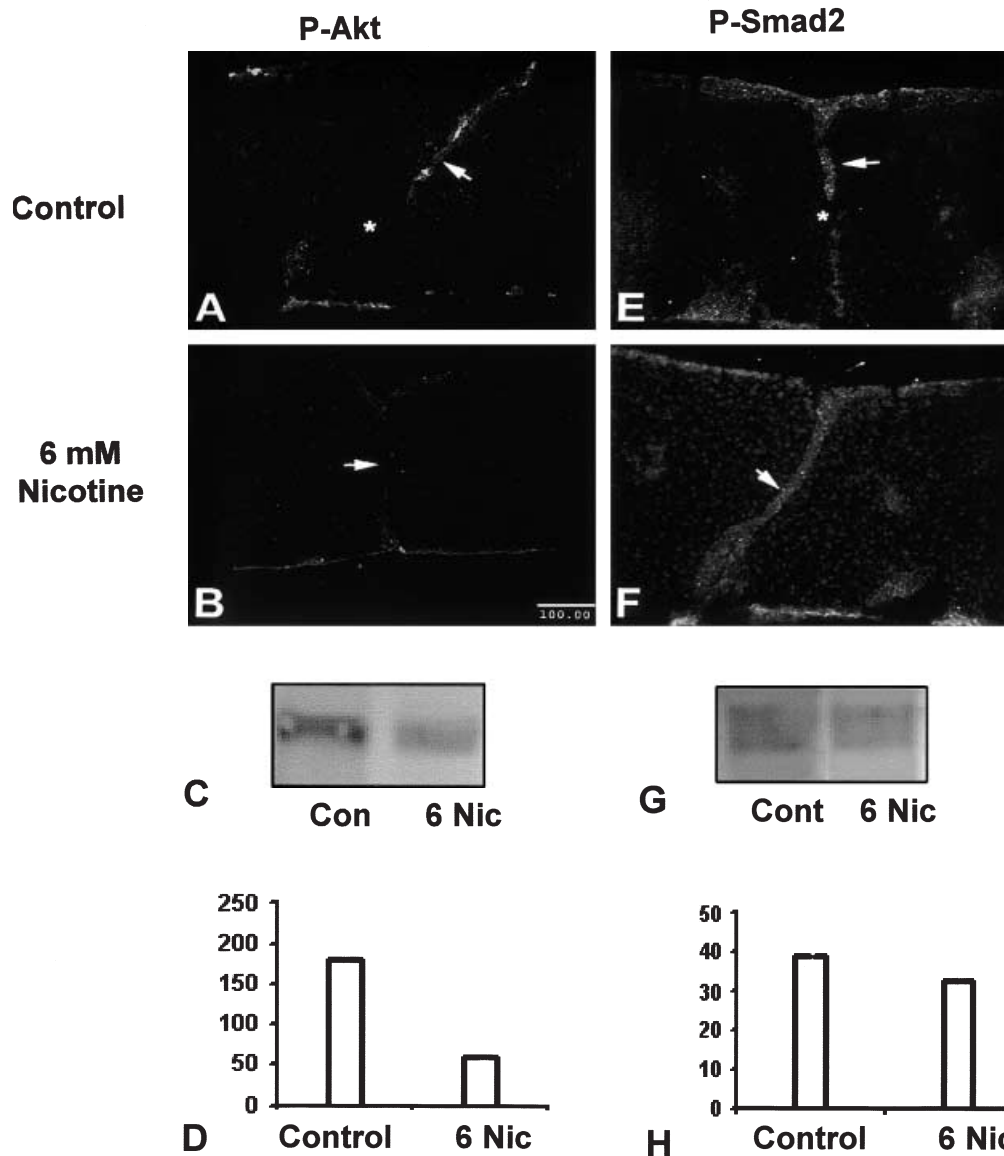


Fig. 3. Immunohistochemical (A–F) and protein analysis (C and G) of phosphorylated Akt (Ser 473) (A–D) and phosphorylated Smad2 (Ser 465/467) (E–H). Tissues were cultured with (B and F) or without (A and E) 6 mM nicotine and harvested at 20 h. Images were obtained with a Leica SP2 confocal microscope set at the same settings on the same day for all samples for comparison of relative intensity. The control medial edge epithelia (arrow, A and E) were positive for both phosphorylated Akt and Smad2. Areas that had progressed through EMT were negative for both proteins (*, A and E). In palates treated with 6 mM nicotine the phosphorylated Akt was decreased in the medial epithelia (arrow, B) but the phosphorylated Smad2 was similar to controls (arrow, F). Western blots of the medial epithelial region (n = 15 palates pooled/treatment group/experiment) were compared between controls (Con) and nicotine treated palates (6 Nic). Data from duplicate experiments were analyzed by densitometry (D and H) to demonstrate that the decrease in phosphorylated Akt was consistent, however, no difference in phosphorylated Smad2 was detectable with either immunohistochemistry or protein biochemistry. Error bars indicate standard deviations. Intensities were shown in relative optical densities. Scale bar = 100 μ M.

Nicotinic acetylcholine receptor analysis

α -Bungarotoxin irreversibly binds many subunits of nAChRs with high affinity and blocks their activation. Fluorescent α -bungarotoxin (α -BTX) was used to determine the localization of nAChRs in palate tissues. Cryostat cross-sections from embryonic mouse palates cultured for 20 h were evaluated. Fluorescent α -BTX

was observed in the nasal (n), oral (o), and midline epithelia (mee) (arrows, Fig. 4A) of the E14.5-day *in vivo* mouse palate during normal fusion. Staining was not continuous along the midline (asterisks, Fig. 4A), suggesting that some MEE transformed into mesenchyme and no longer expressed the midline epithelial protein, nAChRs. The location and intensity of fluorescent α -BTX in the palates cultured under

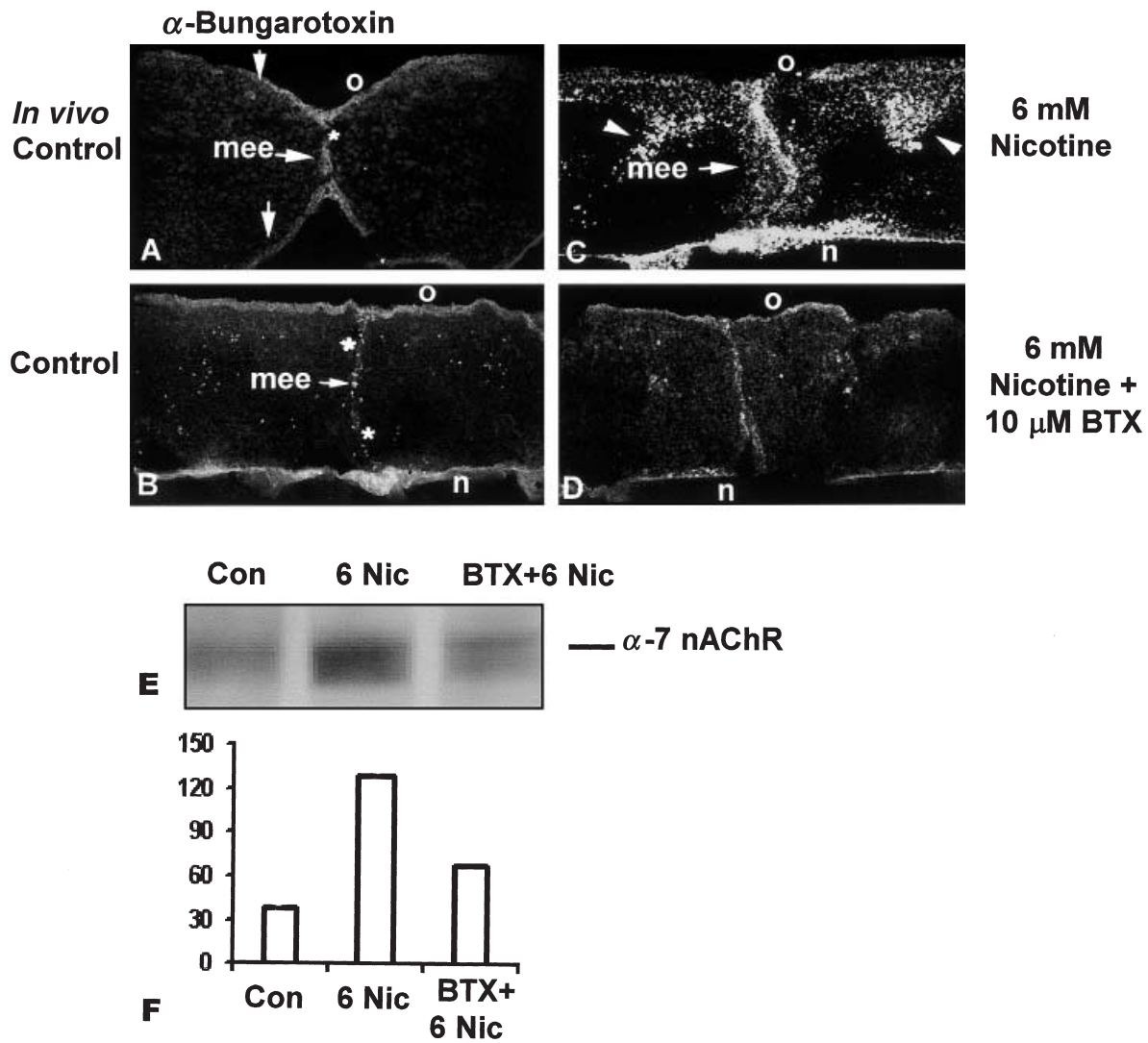


Fig. 4. Fluorescent α -bungarotoxin labeled frozen sections (A–D) and western blot analysis (E–F) for the α -7 nAChR subunit in palate. Palatal tissues were obtained either from E 14.5 *in vivo* embryos (A) or from palates cultured for 20 h in control medium (B), 6 mM nicotine (C), or 6 mM nicotine and 10 μ M α -bungarotoxin (α -BTX) (D). Images were obtained with a Leica SP2 confocal microscope set at the same settings on the same day for all samples for comparison of relative intensity. Fluorescent α -bungarotoxin bound to the oral, nasal and MEE in all palates examined (arrows, A–C), however it was more intense and also present on mesenchymal cells in nicotine treated palates (arrowheads, C). Treating the palates with both nicotine and α -bungarotoxin decreased binding (D). Western blots of the medial epithelial region ($n = 15$ palates pooled/treatment group/experiment) for the α -7 nAChR were compared between controls (Con), nicotine treated palates (6 Nic), and 10 μ M α -bungarotoxin + nicotine (BTX+6 Nic) (E). Data from duplicate experiments were analyzed by densitometry (F) to demonstrate that the nicotinic receptor subunit increased in the presence of nicotine and decreased in the presence of 10 μ M α -BTX and nicotine. Error bars indicate standard deviations. Intensities were shown in relative denominations. Medial edge epithelia (mee), oral surface (o), nasal surface (n).

control conditions were similar to E14.5 mouse palates (arrow, Fig. 4B), with more gaps in MEE (asterisks, Fig. 4B). In the 6 mM nicotine treated palates, however, the staining was continuous in the fusion zone and the intensity was greater in the epithelia, especially in MEE, than the control cultured palates (arrow, Fig. 4C). In addition, the mesenchymal cells and other areas were intensely labeled lateral to the MEE (arrowheads, Fig. 4C). Some of these areas also stained with laminin, indicating that they may be epithelial cell populations

(data not shown). This pattern of nAChR localization was not observed in control-cultured samples (Fig. 4B).

The α -7 nicotinic receptor subunit is one of the nAChRs expressed in epithelia and is selectively, irreversibly bound by α -BTX (41, 50, 51). Western blot analysis demonstrated that α -7 nAChR subunit increased 3.3-fold in tissues treated with nicotine (6 Nic Fig. 4E) compared with control tissues (Con, Fig. 4E) quantified by densitometry from duplicate experiments (Fig. 4F).

Addition of nicotinic receptor antagonists decreased the level of nAChRs, but did not rescue the non-fusion effect of nicotine

To investigate if nicotine inhibited palate fusion by directly binding to nAChRs, culture media was supplemented with 1 μM or 10 μM α -BTX, with or without 6 mM nicotine. Tissues treated with 1 or 10 μM α -BTX fused after 72 h in culture except for two stage 3 (partial) fusions (Table 1). The tissue morphology resembled those of control-cultured palates (Fig. 1D, G). Only a few discrete fluorescent islands were observed in a single optical image of CCFSE labeled whole mount palate (arrows, Fig. 5A). There were no epithelia remaining in the fusion zone in H and E stained sections (Fig. 5B). The combination of 6 mM nicotine and α -BTX did not rescue the palates from non-fusion, although two of 12 samples were partially fused (Table 1). The CCFSE labeled MEE were continuous anterior-posteriorly (Fig. 5B) and two layers of epithelia persisted in the fusion zone (arrows, Fig. 5D).

The location and intensity of fluorescent α -BTX staining of the samples treated with the combination of 6 mM nicotine and α -BTX (Fig. 4D) were similar to control palates (Fig. 4B). Western blot analysis showed a decrease in α -7 nAChR subunit compared with nicotine treated tissues, although the level was higher than control samples analyzed from duplicate experiments (BTX+6 Nic, Fig. 4E).

Discussion

Using lipophilic cellular markers (DiI or CCFSE) or retroviral vectors, several research groups traced the fate of MEE (20, 21, 43, 52). These experiments concluded that the majority of MEE, if not all, remain in the tissue but go through cellular changes and obtain mesenchymal characteristics. In our study, CCFSE (43) was used to label the surface epithelia before culture. The CCFSE diffuses through the cell membrane, and intracellular esterase cleaves the acetates to release the fluorophore. The product is packaged into intracellular compartments as a lipid insoluble compound, which can pass through gap junctions into the basal layer but does not get into the underlying mesenchyme. Therefore, it exclusively labels the epithelial cell population. The direct entry of CCFSE into periderm enables this epithelial layer to be more intensely labeled than the basal MEE (53). During *in vitro* palate fusion, peridermal cells go through apoptosis (18). This would explain why the intensity of CCFSE labeling in our completely fused palatal cultures was low. Other studies have suggested that there may be dye spreading during sectioning of tissues labeled using DiI or CCFSE (54). In these experiments, the potential dye spreading was avoided by analyzing whole-mount tissues with confocal microscopy. The current experiments clearly demonstrated that CCFSE labeled epithelial cells and

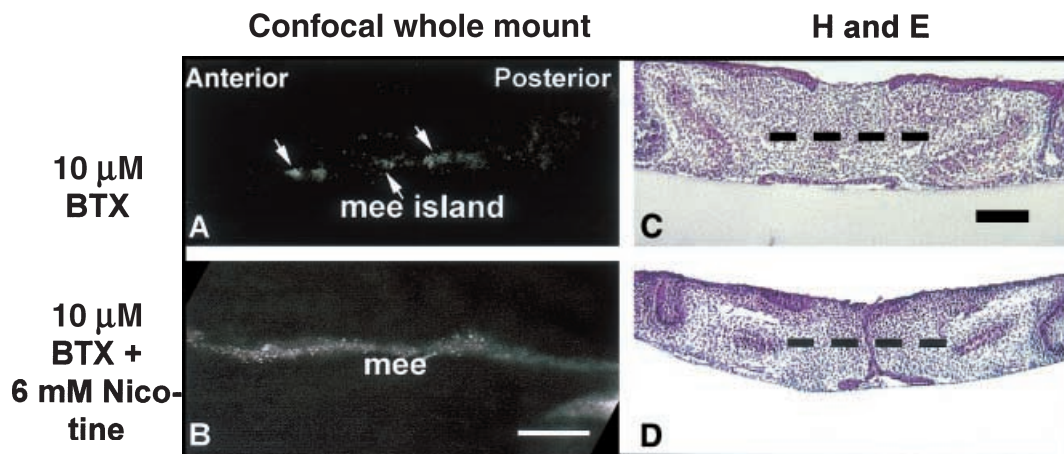


Fig. 5. Analysis of palates after 72 h of culture in 10 μM α -bungarotoxin without nicotine (A and C) or with nicotine (B and D). (A and B) Single optical confocal sections through carboxy 2,7' dichlorofluorescein diacetate succinimidyl ester (CCFSE) labeled whole mount palatal tissues in the middle of the tissue, 120 μm from the oral surface. The α -bungarotoxin treated palates had transformed medial edge epithelia (MEE) demonstrated by decreased CCFSE staining with some islands remaining in the midline (arrows, A) and lack of midline epithelia in H and E stained sections (C), whereas, the tissues treated with both bungarotoxin and 6 mM nicotine had persistent MEE in both CCFSE analyzed tissues (B) and H and E sections (D). Scale bar = 200 μm in A and B, =100 μm in C and D.

the mesenchyme formed confluence after 72 h of culture in control conditions.

The amount of phosphorylated Smad2 in the MEE of 20-h nicotine treated palates did not change compared with controls. The immunohistochemistry demonstrated that Smad2 was approximately the same in controls and nicotine treated MEE, but more MEE cells remained in the midline of the nicotine treated palates (Fig. 3).

A previous study in our lab demonstrated that the inhibition of PI-3 kinase activity by LY 294002 resulted in the failure of EMT and palatal fusion (33). The mechanisms suggested were: (1) PI-3 kinase may be involved in initiation of palatal fusion through new desmosome formation; (2) PI-3 kinase may regulate basement membrane degradation by modulating MMP production; (3) PI-3 kinase may be downstream of TGF β 3 during palate fusion. In addition, ILK may be a signaling molecule downstream of PI-3 kinase regulating EMT (47, 48). Activated ILK phosphorylates its downstream effector Akt on the serine 473 site. Therefore, we examined the level of phosphorylated Akt (Ser473) and demonstrated that it was significantly decreased in the 6 mM nicotine treated tissues after 20 h, suggesting nicotine may have inhibited EMT and palatal fusion through interference with the PI-3 kinase pathway.

The receptors in cholinergic transmission are composed of the muscarinic acetylcholine receptors, which are G-coupled receptors; and the nAChRs. The neuronal nAChRs are a family of ACh-gated ion channels consisting of eight α and three β subunits and are also present in non-neuronal cells, including keratinocytes (51, 55). Addition of ACh or nicotine to cultured human keratinocytes modifies their proliferation, differentiation, and motility (40, 41, 50), suggesting the presence of functional nAChRs in keratinocytes. An interesting aspect of nAChR regulation is that chronic exposure to nicotine can result in an increase in the number of nAChRs as observed in the human brains of tobacco smokers (56, 57). The regulation of nAChRs is in contradiction with the general rule that over-exposure to agonists decreases the number of receptors. Depending on the nature of the agonist and the length of exposure, nAChRs go through rapid reversible desensitization, permanent inactivation, and post-transcriptional up regulation to compensate for the non-functional receptors (58–60). This regulation mechanism also

explains the biphasic effects of nicotine on keratinocytes. Addition of ACh or nicotine at 0.1 to 10 mM increased keratinocyte adhesion and migration within 30 min in culture (61), but long-term exposure resulted in up regulated α 7 nAChR subunit and decreased keratinocyte migration (50). It was suggested that α 4, β 2 and α 7 nAChR subunits are more sensitive to up regulation and desensitization (62, 63). We detected nAChRs in the mouse palate MEE using fluorescent α -BTX. Our results from protein analysis suggested that the α 7 nAChR subunit increased in tissues treated with 6 mM nicotine for 20 h. These data lead to the speculation that normal functions of nAChRs are essential during EMT in palate development; while an overdose of nicotine resulted in inactivated although up regulated nAChRs.

Two possible reasons may explain why α -BTX did not rescue palatal non-fusion. First, the concentration of α -BTX may have been too low in relation to the dosage of nicotine. In a recent study (64) 1 μ M α -BTX was used to reverse the effects of 10 μ M nicotine in keratinocyte cultures. In contrast, in this study 10 μ M α -BTX was applied to palates that were treated with 6 mM nicotine. Secondly, nAChRs may be required for EMT and palatal fusion as antagonist treatment resulted in inactivation of the receptors. Although α -BTX treatment alone did not inhibit palatal fusion, addition of either *d*-tubocurarine or mecamylamine at 1 mM concentration in culture media resulted in partial fusion or non-fusion of the palates with MFS of 3.0 and 3.71, respectively (data not shown). Supporting our hypothesis that nAChRs may be required for EMT and palatal fusion. The observation that α -BTX alone did not inhibit fusion can be explained as (i) α -BTX is a very specific nAChR antagonist and only blocks the activation of homomeric α 7, α 8, and α 9 subunits (51), and (ii) the highest concentration used was 10 μ M instead of millimolar concentrations. In addition, mice produced with a substitution of a threonine for a leucine at position 247 in the channel domain have reduced levels of α 7 nAChR and die shortly after birth because of neurological problems, however they do not have cleft palates (65).

In neural cell cultures, α 7-receptor subunit associates with the PI-3 kinase p85 subunit, stimulates Ca²⁺ influx, and activates Akt (66). If this is also true in epithelia, it is possible that the nicotine inactivation of nAChRs in the MEE inhibited EMT and fusion through the PI-3 kinase - Akt pathway.

Other *in vitro* studies also used millimolar nicotine concentrations (50). These nicotine concentrations were significantly higher than the level of nicotine found in the arterial blood from smokers and may not be relevant to an *in vivo* situation. Although these experiments did not examine the possible function of nicotine metabolites, such as cotinine, they clearly demonstrated that nicotine inhibited palatal fusion *in vitro*. The decreased active Akt and increased $\alpha 7$ nAChR subunits may suggest that the PI-3 kinase pathway may be down stream of nAChR signaling for EMT during palate fusion.

Acknowledgements: We thank Jesus Acevedo, Tamara Field, Jan Lalor, Steve Lin and Petra Moessner for their technical assistance. We are also grateful to the Baylor Oral Health Foundation, Tobacco Endowment Fund, and NIH EY08886 for supporting the study.

References

- Abel EL. Smoking during pregnancy: a review of effects on growth and development of offspring. *Hum Biol* 1980;**52**:593–625.
- Rowell PP, Clark MJ. The effect of chronic oral nicotine administration on fetal weight and placental amino acid accumulation in mice. *Toxicol Appl Pharm* 1982;**66**:30–8.
- Tuthill DP, Stewart JH, Coles EC, Andrews J, Cartledge PH. Maternal cigarette smoking and pregnancy outcome. *Paed & Perinat Epidemiol* 1999;**13**:245–53.
- Seller MJ, Bnait KS, Cairns NJ. Effect of maternal tobacco smoke inhalation on early embryonic growth. In: Poswillo D, Alberman E, editors. *Effects of Smoking on the Fetus, Neonate and Child*. Oxford: Oxford University Press; 1992. pp. 45–59.
- Gartner LP, Saad AY, Hiatt JL. Effects of nicotine on murine incisor development. *J Biol Buccale* 1990;**18**:83–8.
- Saad AY, Gartner LP, Hiatt JL. Teratogenic effects of nicotine on first molar odontogenesis in the mouse. *Acta Morphol Hung* 1991;**39**:87–96.
- Gartner LP, Saad AY, Hiatt JL. Effects of nicotine on tongue development in the cd-1 mouse. *Eur J Morphol* 1997;**35**:337–43.
- Hwang SJ. Association study of transforming growth factor alpha (TGF alpha) taqi polymorphism and oral clefts: indication of gene–environment interaction in a population-based sample of infants with birth defects. *Amer J Epidemiol* 1992;**135**:1000–11.
- Chung KC, Kowalski CP, Kim HM, Buchman SR. Maternal cigarette smoking during pregnancy and the risk of having a child with cleft lip/palate. *Plast Reconstr Surg* 2000;**105**:485–91.
- Lorente C, Cordier S, Goujard J, Ayme S, Bianchi F, Calzolari E et al. Tobacco and alcohol use during pregnancy and risk of oral clefts. Occupational exposure and congenital malformation working group. *Am J Public Health* 2000;**90**:415–9.
- Weinzweig J, Panter KE, Pantaloni M, Spangenberg A, Harper JS, Lui F et al. The fetal cleft palate: I. Characterization of a congenital model. *Plast Reconstr Surg* 1999;**103**:419–28.
- Panter KE, Weinzweig J, Gardner DR, Stegelmeier BL, James LF. Comparison of cleft palate induction by nicotiana glauca in goats and sheep. *Teratology* 2000;**61**:203–10.
- Saad AY, Gartner LP, Hiatt JL. Teratogenic effects of nicotine on palate formation in mice. *Biol Struct Morph* 1990;**3**:31–5.
- Idoyaga-Vargas V, Nasjleti CE, Azcurra JM. Cytodifferentiation of the mouse secondary palate in vitro: morphological, biochemical, and histochemical aspects. *J Embryol Exp Morphol* 1972;**27**:413–30.
- Tyler MS. In vitro development of palatal tissues from embryonic mice. I. Differentiation of the secondary palate from 12-day mouse embryos. *Anat Rec* 1975;**182**:297–301.
- Ferguson MW. Palate development. *Develop* 1988;**103**(Suppl): 41–60.
- Waterman RE, Meller SM. Alterations in the epithelial surface of human palatal shelves prior to and during fusion: a scanning electron microscopic study. *Anat Rec* 1974;**180**:111–35.
- Fitchett JE, Hay ED. Medial edge epithelium transforms to mesenchyme after embryonic palatal shelves fuse. *Dev Biol* 1989;**131**:455–74.
- Kaufman MH. *The Atlas Of Mouse Development*, 2nd edn. San Diego: Academic Press; 1995. pp. 425–34.
- Martinez-Alvarez C, Tudela C, Perez-Miguelsanz J, O’Kane S, Puerta J, Ferguson MW. Medial edge epithelial cell fate during palatal fusion. *Dev Biol* 2000;**220**:343–57.
- Shuler CF, Halpern DE, Guo Y, Sank AC. Medial edge epithelium fate traced by cell lineage analysis during epithelial-mesenchymal transformation in vivo. *Dev Biol* 1992;**154**:318–30.
- Kaartinen V, Voncken JW, Shuler C, Warburton D, Bu D, Heisterkamp N et al. Abnormal lung development and cleft palate in mice lacking tgf-beta 3 indicates defects of epithelial-mesenchymal interaction. *Nat Genet* 1995;**11**:415–21.
- Proetzel G, Pawlowski SA, Wiles MV, Yin M, Boivin GP, Howles PN et al. Transforming growth factor- $\beta 3$ is required for secondary palate fusion. *Nat Genet* 1995;**11**:409–14.
- Kaartinen V, Cui XM, Heisterkamp N, Groffen J, Shuler CF. Transforming growth factor-beta3 regulates transdifferentiation of medial edge epithelium during palatal fusion and associated degradation of the basement membrane. *Dev Dyn* 1997;**209**:255–60.
- Taya Y, O’Kane S, Ferguson MW. Pathogenesis of cleft palate in tgf-beta3 knockout mice. *Develop* 1999;**126**:3869–79.
- Cui XM, Warburton D, Zhao J, Crowe DL, Shuler CF. Immunohistochemical localization of tgf-beta type II receptor and tgf-beta3 during palatogenesis in vivo and in vitro. *Int J Dev Biol* 1998;**42**:817–20.
- Sun D, Vanderburg CR, Odierna GS, Hay ED. TGF $\beta 3$ promotes transformation of chicken palate medial edge epithelium to mesenchyme in vitro. *Develop* 1998;**125**:95–105.
- Attisano L, Wrana JL. Smads as transcriptional co-modulators. *Curr Opin Cell Biol* 2000;**12**:235–43.
- Miyazono K. TGF- β signaling by Smad proteins. *Cytok Grow Fac Rev* 2000;**11**:15–22.
- Cui XM, Chai Y, Ito Y, Shuler CF. Expression of T β R-I and Smad2 in embryonic palatal tissues. *J Dent Res* 2000;**79**(IADR abstracts):416.
- Metzner B, Barbisch M, Bachmann F, Czech W, Norgauer J. Evidence of the involvement of phosphatidylinositol 3-kinase in the migration, actin stress fiber formation, and alpha v beta 3-integrin-mediated adherence of human melanoma cells. *J Invest Dermatol* 1996;**107**:597–602.
- Sugiura T, Berditchevski F. Function of alpha 3 beta 1-tetraspanin protein complexes in tumor cell invasion. Evidence for the role of the complexes in production of matrix metalloproteinase 2 (MMP-2). *J Cell Biol* 1999;**146**:1375–89.

33. Kang P, Svoboda KKH. PI-3 kinase activity is essential for epithelial-mesenchymal transformation during murine palate fusion. *Dev Dyn* 2002;**225**:316–21.
34. Carty CS, Soloway PD, Kayastha S, Bauer J, Marsan B, Ricotta JJ et al. Nicotine and cotinine stimulate secretion of basic fibroblast growth factor and affect expression of matrix metalloproteinases in cultured human smooth muscle cells [Erratum appears in *J Vasc Surg* 1997 Apr;25(4):628]. *J of Vas Surg* 1996;**24**:927–34; Discussion 934–5.
35. Cucina A, Sapienza P, Corvino V, Borrelli V, Mariani V, Randone B et al. Nicotine-induced smooth muscle cell proliferation is mediated through bFGF and TGF-beta 1. *Surg* 2000;**127**:316–22.
36. Cucina A, Corvino V, Sapienza P, Borrelli V, Lucarelli M, Scarpa S et al. Nicotine regulates basic fibroblastic growth factor and transforming growth factor beta1 production in endothelial cells. *Biochem Biophys Res Commun* 1999;**257**:306–12.
37. Mathur RS, Mathur SP, Young RC. Up-regulation of epidermal growth factor-receptors (EGF-R) by nicotine in cervical cancer cell lines: this effect may be mediated by egf. *Am J Reprod Immunol* 2000;**44**:114–20.
38. Rakowicz-Szulczynska EM, McIntosh DG, Smith M. Growth factor-mediated mechanisms of nicotine-dependent carcinogenesis. *Carcinogenesis* 1994;**15**:1839–46.
39. Nguyen VT, Ndoye A, Grando SA. Pemphigus vulgaris antibody identifies pemphaxin. A novel keratinocyte annexin-like molecule binding acetylcholine. *J Biol Chem* 2000;**275**:29 466–76.
40. Grando SA, Horton RM, Pereira EF, Diethelm-Okita BM, George PM, Albuquerque EX et al. A nicotinic acetylcholine receptor regulating cell adhesion and motility is expressed in human keratinocytes. *J Invest Dermatol* 1995;**105**:774–81.
41. Zia S. Receptor-mediated inhibition of keratinocyte migration by nicotine involves modulations of calcium influx and intracellular concentration. *J Pharm & Exper Therap* 2000;**293**:973–81.
42. Grando SA. Activation of keratinocyte nicotinic cholinergic receptors stimulates calcium influx and enhances cell differentiation. *J Invest Dermatol* 1996;**107**:412–8.
43. Griffith CM, Hay ED. Epithelial-mesenchymal transformation during palatal fusion: carboxyfluorescein traces cells at light and electron microscopic levels. *Develop* 1992;**116**:1087–99.
44. Hay ED. An overview of epithelio-mesenchymal transformation. *Acta Anat* 1995;**154**:8–20.
45. Le Good JA, Ziegler WH, Parekh DB, Alessi DR, Cohen P, Parker PJ. Protein kinase C isotypes controlled by phosphoinositide 3-kinase through the protein kinase PDK1. *Science* 1998;**281**:2042–5.
46. Alessi DR, Kozlowski MT, Weng QP, Morrice N, Avruch J. 3-phosphoinositide-dependent protein kinase 1 (PDK1) phosphorylates and activates the p70 S6 kinase in vivo and in vitro. *Curr Biol* 1998;**8**:69–81.
47. Kang P, Svoboda KKH. Epithelial-mesenchymal transformation during palate fusion requires PI3 kinase activity. *Mol Biol Cell* 2000;**11**(Suppl):60a.
48. Radeva G, Petrocelli T, Behrend E, Leung-Hagesteijn C, Filmus J, Slingerland J et al. Overexpression of the integrin-linked kinase promotes anchorage-independent cell cycle progression. *J Biol Chem* 1997;**272**:13 937–44.
49. Wu C, Keightley SY, Leung-Hagesteijn C, Radeva G, Coppolino M, Goicoechea S et al. Integrin-linked protein kinase regulates fibronectin matrix assembly, E-cadherin expression, and tumorigenicity. *J Biol Chem* 1998;**273**:528–36.
50. Zia S. Nicotine enhances expression of the alpha 3, alpha 4, alpha 5, and alpha 7 nicotinic receptors modulating calcium metabolism and regulating adhesion and motility of respiratory epithelial cells. *Res Comm Mol Path & Pharm* 1997;**97**:243–62.
51. Gotti C, Fornasari D, Clementi F. Human neuronal nicotinic receptors. *Prog Neurobiol* 1997;**53**:199–237.
52. Shuler CF, Guo Y, Majumder A, Luo RY. Molecular and morphologic changes during the epithelial-mesenchymal transformation of palatal shelf medial edge epithelium in vitro. *Int J Dev Biol* 1991;**35**:463–72.
53. Sun D, Baur S, Hay ED. Epithelial-mesenchymal transformation is the mechanism for fusion of the craniofacial primordia involved in morphogenesis of the chicken lip. *Dev Biol* 2000;**228**:337–49.
54. Garton HJ, Schoenwolf GC. Improving the efficacy of fluorescent labeling for histological tracking of cells in early mammalian and avian embryos. *Anat Rec* 1996;**244**:112–17.
55. Sastry BV. Cholinergic systems in non-nervous tissues. *Pharm Rev* 1978;**30**:65–132.
56. Benwell ME. Evidence that tobacco smoking increases the density of (-)-[3H]nicotine binding sites in human brain. *Biochem Soc Trans* 1990;**18**:885–6.
57. Wonnacott S. The paradox of nicotinic acetylcholine receptor upregulation by nicotine. *Trend Pharm Sci* 1990;**11**:216–9.
58. Schwartz RD. In vivo regulation of [3H]acetylcholine recognition sites in brain by nicotinic cholinergic drugs. *J Neurochem* 1985;**45**:427–33.
59. Marks MJ. Nicotine binding and nicotinic receptor subunit rna after chronic nicotine treatment. *J Neurosci* 1992;**12**:2765–84.
60. Reitsstetter R. Dependence of nicotinic acetylcholine receptor recovery from desensitization on the duration of agonist exposure. *J Pharm & Exp Therap* 1999;**289**:656–60.
61. Grando SA. Keratinocyte muscarinic acetylcholine receptors: immunolocalization and partial characterization. *J Invest Dermatol* 1995;**104**:95–100.
62. Hsu YN. Sustained nicotine exposure differentially affects alpha 3 beta 2 and alpha 4 beta 2 neuronal nicotinic receptors expressed in xenopus oocytes. *J Neurochem* 1996;**66**:667–75.
63. Olale F. Chronic nicotine exposure differentially affects the function of human alpha3, alpha4, and alpha7 neuronal nicotinic receptor subtypes. *J Pharm & Exp Therap* 1997;**283**:675–83.
64. Arredondo J, Nguyen VT, Chernyavsky AI, Bercovich D, Orr-Urtreger A, Krummer W et al. Central role of alpha 7 nicotinic receptor in differentiation of the stratified squamous epithelium. *J Cell Biol* 2002;**159**:325–36.
65. Orr-Urtreger A, Broide RS, Kasten MR, Dang H, Dani JA, Beaudet AL et al. Mice homozygous for the L250T mutation in the alpha 7 nicotinic acetylcholine receptor show increased neuronal apoptosis and die within one day of birth. *J Neurochem* 2000;**74**:2154–65.
66. Kihara T, Shimohama S, Sawada H, Honda K, Nakamizo T, Shibasaki H et al. Alpha 7 nicotinic receptor transduces signals to phosphatidylinositol 3-kinase to block a beta-amyloid-induced neurotoxicity. *J Biol Chem* 2001;**276**:13 541–6.